Pharmaceutical Research, Vol. 25, No. 5, May 2008 (© 2007)
DOI: 10.1007/s11095-007-9446-6

Research Paper

Multiple Inhibition Mechanisms and Prediction of Drug–Drug Interactions: Status of Metabolism and Transporter Models as Exemplified by Gemfibrozil–Drug Interactions

Laura K. Hinton,[1] Aleksandra Galetin,[1,2] and J. Brian Houston[1]

Received May 10, 2007; accepted August 28, 2007; published online September 27, 2007

Purpose. To assess the consequences of multiple inhibitors and differential inhibition mechanisms on the prediction of 12 gemfibrozil drug–drug interactions (DDIs). In addition, qualitative zoning of transporter-related gemfibrozil and cyclosporine DDIs was investigated.
Methods. The effect of gemfibrozil and its acyl-glucuronide on different enzymes was incorporated into a metabolic prediction model. The impact of CYP2C8 time-dependent inhibition by gemfibrozil acyl-glucuronide was assessed using repaglinide, cerivastatin, loperamide, rosiglitazone and pioglitazone DDIs. Gemfibrozil and cyclosporine inhibition data obtained in human embryonic kidney cells expressing OATP1B1 and hepatic input concentration ([*I*]in) were used for qualitative zoning of 14 transporter-mediated DDIs.
Results. Incorporation of time-dependent inhibition by gemfibrozil glucuronide showed no significant improvement in the prediction, as CYP2C8 contributed <65% to the overall elimination of the victim drugs investigated. Qualitative zoning of OATP1B1 DDIs resulted in no false negative predictions; yet the magnitude of observed interactions was significantly over-predicted.
Conclusions. Time-dependent inhibition by gemfibrozil glucuronide is only important for victim drugs eliminated predominantly (>80%) via CYP2C8. Qualitative zoning of OATP1B1 inhibitors based on [*I*]in/K_i is valid in drug screening to avoid false negatives. Refinement of the transporter model by incorporating the fraction of drug transported by a particular transporter is recommended.

KEY WORDS: CYP2C8; drug–drug interactions; enzyme inhibition; gemfibrozil; OATP1B1.

In vitro–in vivo prediction approaches for metabolic reversible and irreversible drug–drug interactions (DDIs) have been extensively evaluated in recent years (1–4). The metabolic prediction models focus on inhibition of P450 enzymes and have undergone several refinements to improve their accuracy, including incorporation of parallel elimination pathways (defined by fraction of drug metabolised, fm_{CYPi}), use of various plasma inhibitor concentrations as surrogates for inhibitor concentration at the enzyme active site, use of K_i values obtained under standardised *in vitro* conditions and incorporation of inhibition of intestinal metabolism (5–9). However, these models have been largely restricted to considering one inhibitory mechanism and one particular inhibitory drug.

DDIs involving the lipid-regulating agent gemfibrozil have received much attention in recent years and provide a major challenge to our current ability to predict from *in vitro* systems. Both gemfibrozil and its major metabolite, gemfibrozil 1-*O*-β-glucuronide, are *in vitro* inhibitors of CYP2C8 and the hepatic uptake transporter OATP1B1 (10–12); in both cases the acyl-glucuronide is the more potent inhibitor. In addition, gemfibrozil shows greater inhibition potency towards CYP2C9 *in vitro* in comparison to CYP2C8 (13) and is a weak CYP3A4 inhibitor (14). An apparent discrepancy between *in vitro* and *in vivo* inhibition exists as the major DDIs observed *in vivo* have been with CYP2C8 or mutual CYP2C8/CYP3A4 substrates rather than CYP2C9 (15–18). The most pronounced gemfibrozil interactions were observed with repaglinide (16) and cerivastatin (15) (mean increase in AUC of 8.1 and 5.6, respectively), whereas gemfibrozil has minimal effect on glimepiride (19) and atorvastatin AUC (20). An additional characteristic of the gemfibrozil interactions is the substantial inter-individual variability in the

[1] School of Pharmacy and Pharmaceutical Sciences, University of Manchester, Stopford Building, Oxford Road, Manchester, M13 9PT, UK.
[2] To whom correspondence should be addressed. (e-mail: Aleksandra.Galetin@manchester.ac.uk)

ABBREVIATIONS: AUC, area under the plasma concentration–time curve; AUCi, area under the curve in the presence of the inhibitor; DDI, drug–drug interactions; fm_{CYPi}, fraction of drug metabolised by the particular P450 enzyme subject to inhibition; F+, F−, false positive and false negative predictions; ft, the fraction of drug transported by a particular transporter protein; [*I*], inhibitor concentration; [*I*]in, hepatic input concentration; K_I, inhibitor concentration at 50% of k_{inact}; K_i, inhibition constant; k_{deg}, enzyme degradation rate constant; k_{inact}, maximal inactivation rate constant; TDI, time-dependent inhibition.

inhibitory response observed, as illustrated by the 1.4 to 10-fold increase in the AUC in cerivastatin interaction.

In a recent study Ogilvie *et al.* (21) indicated that the acyl-glucuronide of gemfibrozil is hydroxylated at a distal site to the glucuronide moiety and the formation of this hydroxy-glucuronide results in the inhibition of CYP2C8 in a time-dependent, rather than a reversible manner. Therefore, one aim of this work was to investigate whether the incorporation of time-dependent inhibition (TDI) of CYP2C8 in a metabolic prediction model would account for the discrepancy in potency of gemfibrozil inhibition observed *in vitro* and *in vivo*. The impact of multiple inhibitors and multiple inhibition mechanisms are addressed using gemfibrozil interactions with victim drugs with a differential contribution of CYP2C8 to their elimination.

A number of recent studies (22–25) have indicated the importance of the hepatic uptake transporter OATP1B1 on the disposition and efficacy of the drugs investigated here for interactions with gemfibrozil. The members of organic anion-transporting polypeptides (OATP) mediate the uptake of a number of compounds that vary in physico-chemical properties ranging from hydrophilic (pravastatin, rosuvastatin) to lipophilic (e.g., repaglinide). Therefore, inhibition of the hepatic uptake of the victim drugs may contribute towards the observed extent of a DDI. Prediction of DDIs occurring via hepatic transporter proteins is currently based on an approach analogous to the basic metabolic model using the ratio of the inhibitor concentration [*I*] and the inhibition constant (K_i) (11). This approach assumes that transport occurs exclusively via the particular transport protein subject to inhibition and that no passive uptake occurs.

In the current study, inhibition data obtained for gemfibrozil and cyclosporine in human embryonic kidney cells (HEK293) expressing OATP1B1 were used to evaluate $[I]/K_i$ ratio as a pragmatic way to qualitatively zone 14 transporter-related gemfibrozil and cyclosporine drug–drug interactions. The cyclosporine studies were included for comparative purposes, as it is a well-known, potent inhibitor of OATP1B1. Hepatic input concentration ([*I*]in) was selected based on a previous study involving qualitative zoning of potential reversible metabolic inhibitors (2) where [*I*]in was most successful in eliminating false negative predictions. The [*I*]in value combines the circulating systemic plasma concentration and the concentration of an inhibitor occurring during the absorption phase. In addition, to increase the quantitative value of DDI predictions, we propose a refinement of the basic transporter model and the incorporation of a substrate-specific property. This additional term, the fraction of drug transported by a particular transporter protein (ft), is analogous to fm_{CYPi} in the metabolic prediction model (see Appendix). The impact of this victim drug-specific parameter on the prediction of transporter-related DDIs is assessed over a range of inhibitor potencies.

MATERIALS AND METHODS

Database of gemfibrozil interactions. A database of gemfibrozil DDIs was collated and the impact of multiple inhibitors (gemfibrozil and its glucuronide) and different inhibition mechanisms of CYP2C8 (reversible and time-dependent) were investigated for a range of victim drugs with differential contributions from CYP3A4, CYP2C8 and CYP2C9 to their elimination, as illustrated in Table I. The area under the plasma concentration–time profile in the presence relative to the absence of the inhibitor (AUCi/AUC) was used as the metric to measure the extent of interaction (1,2). In the case of replicate studies (same dosing regimens) the average AUCi/AUC was calculated as a weighted mean as described previously (6). In the DDI studies included in the database, multiple oral doses of inhibitors were administered (assuming steady-state was reached) before the second administration of the substrate.

The role of metabolic, relative to hepatic uptake, inhibition was investigated by comparing the changes in the apparent volume of distribution (V/F) and oral clearance (CL) of the substrates in the presence of gemfibrozil. The V/F and CL of each of the substrates in the gemfibrozil interactions were estimated in the absence and presence of the inhibitor (except for lovastatin where the half-life was not

Table I. List of Observed *In Vivo* and Predicted AUCi/AUC Ratios for 12 Drug–Drug Interactions with Gemfibrozil using Reversible or Combined Reversible and TDI Metabolic Models

		Mean AUCi/AUC Predicted				
Victim Drug	Mean Observed AUCi/AUC	Estimated fm_{CYP2C8}	Estimated fm_{CYP2C9}	Estimated fm_{CYP3A4}	Reversible Model[a]	Combined Reversible and TDI[b]
Atorvastatin (20)	1.24	–	–	0.97	1.36	–
Cerivastatin (15)	5.59	0.61	–	0.39	2.40	2.55
Lovastatin (26)	1.78	–	–	0.99	1.37	–
Pioglitazone (27,28)	3.30	0.63	–	0.30	2.52	2.69
Pravastatin (29)	2.02	–	–	0.31	1.09	–
Repaglinide (16)	8.12	0.49	–	0.49	1.89	1.97
Rosiglitazone (30)	2.29	0.50	0.49	–	2.93	3.12
Rosuvastatin (17)	1.88	–	0.36	–	1.20	–
Simvastatin (31)	2.09	–	–	0.99	1.37	–
Glimepiride (19)	1.23	–	0.99	–	1.91	–
Loperamide (32)	2.20	0.38		0.53	1.58	1.62
Zopiclone (33)	0.99			0.95	1.35	

[a,b] Gemfibrozil $[I]_{av,u}$ (3 μM) and the mean estimated unbound hepatic concentration of gemfibrozil-1-*O*-glucuronide (89 μM) were used in metabolic prediction models (Eqs. 3 and 4).

available in both study phases). The assumption was that the inhibitor does not affect the oral bioavailability or plasma protein binding of a victim drug. The percentage change from the control to the inhibitor phase was then calculated. The equations used to estimate volume and clearance are given below.

$$CL = \frac{D}{AUC} \quad (1)$$

$$V/F = \frac{D \times t_{1/2}}{AUC \times 0.693} \quad (2)$$

Metabolic prediction models. The AUCi/AUC ratios for the DDIs involving reversible inhibition of different P450 enzymes (e.g., CYP2C8, CYP2C9 and CYP3A4) by multiple inhibitors (gemfibrozil and its glucuronide) were estimated using the following equation. The model assumes that multiple inhibitors cause inhibition of the enzyme via the same mechanism (3,7).

$$\frac{AUC_i}{AUC} = \frac{1}{\sum_{i}^{n} \frac{fm_{CYP_i}}{1+\sum_{j}^{n} [I]_j / K_{i,j}} + \left(1 - \sum_{i}^{n} fm_{CYP_i}\right)} \quad (3)$$

where fm_{CYPi} represents the fraction of drug metabolised by the particular P450 enzymes subject to inhibition, $(1 - \sum fm_{CYPi})$ represents clearance via other P450 enzymes and/or renal clearance, $[I]$ is the estimated inhibitor concentration ($[I]$av—average plasma concentration during the dosing interval (2)) and K_i is the *in vitro* inhibition constant for the inhibitor against the particular enzyme. The model assumes no inhibition of any additional parallel elimination pathways. Values for fm_{CYPi} (metabolism via CYP3A4, CYP2C8 or CYP2C9) were estimated by urinary recovery of unchanged drug and *in vitro* phenotyping experiments as described previously (5). For the drugs with CYP2C8 and another isoform contributing to their metabolism, the individual fm_{CYP} values were based on *in vitro* studies where the relative contributions were assessed (e.g., pioglitazone, cerivastatin and loperamide (11,34,35)). In cases where these data were unavailable, an equal contribution was assumed (e.g., repaglinide, rosiglitazone). Depending on the differential enzyme contribution, in some instances (e.g., atorvastatin, simvastatin and lovastatin) the equation was simplified and inhibition of only CYP3A4 was considered.

In order to accommodate the effect of multiple inhibitors (gemfibrozil and its glucuronide) via independent inhibition mechanisms (reversible and time-dependent inhibition of CYP2C8, respectively), a modified equation was used:

$$\frac{AUC_i}{AUC} = \frac{1}{\frac{fm_{CYP_i}}{\left(1+\frac{k_{inact} \times [I]_1}{k_{deg} \times (K_I + [I]_1)}\right) \times \left(1 + [I]_2 / K_i\right)} + (1 - fm_{CYP_i})} \quad (4)$$

where k_{deg} is the endogenous degradation rate constant of the enzyme subject to inhibition, k_{inact} is the maximal inactivation rate constant and K_I represents the inhibitor concentration at 50% of the k_{inact} (4). In contrast to Eq. 3, time-dependent inhibition of CYP2C8 by gemfibrozil glucuronide ($[I]_1$) and reversible inhibition of CYP2C8 (or CYP2C9 in the case of rosiglitazone) by gemfibrozil ($[I]_2$) are incorporated in Eq. 4.

Transporter prediction model. The model used for the qualitative zoning of 14 transporter-mediated DDIs is shown in Eq. 5 (11).

$$\frac{AUC_i}{AUC} = 1 + \sum_{i}^{n} [I]/K_i \quad (5)$$

where K_i is obtained as $IC_{50}/2$ assuming competitive inhibition of OATP1B1 hepatic uptake in the presence of gemfibrozil ($n = 8$) and cyclosporine ($n = 6$). Hepatic input concentration ($[I]$in) was used based on the previous success in the qualitative zoning of reversible DDIs (2).

In vitro data. The *in vitro* K_i values for gemfibrozil and its acyl-glucuronide for a range of P450 enzymes are shown in Table II. Gemfibrozil K_i values were corrected using in-house microsomal binding data ($fu_{mic} = 0.53$ at a protein concentration of 1 mg/ml). The K_i values selected have been determined in human liver microsomes with the only exception of the gemfibrozil glucuronide data, where IC_{50} values were obtained using either human liver microsomes or recombinantly expressed P450 enzymes. Gemfibrozil glucuronide IC_{50} values were not corrected for non-specific binding due to the lack of binding data and the assumed hydrophilic nature of this conjugate. The reversible IC_{50} value for gemfibrozil glucuronide may be affected by time-dependent inhibition in the incubation; however, as no pre-incubation step was performed in the original study this would be minimal. Gemfibrozil glucuronide shows a 9-fold

Table II. Gemfibrozil and Gemfibrozil Glucuronide *In Vitro* Data Used in the Metabolism Prediction Models

Inhibitor	Target	*In Vitro* System	K_i (μM)[a]	IC_{50} (μM)	Reference
Gemfibrozil	CYP2C8	Human liver microsomes	69 (36.4)	–	10
	CYP2C9	Human liver microsomes	5.8 (5.3)	–	13
	CYP3A4	Human liver microsomes	–	800 (552)	14
Gemfibrozil-1-*O*-glucuronide[b]	CYP2C8	Recombinant CYP2C8	–	4.1	11
	CYP2C9	Human liver microsomes	300		21
	CYP3A4	Recombinant CYP3A4		243	11

[a] Number in parenthesis refer to gemfibrozil K_i and IC_{50} values corrected for the microsomal binding, $fu_{mic} = 0.53$ at protein concentration of 1 mg/ml.

[b] CYP2C8 k_{deg} of 0.0005–0.00144 min^{-1} (36) and the k_{inact} and K_I values for gemfibrozil glucuronide of 0.21 min^{-1} and 20 μM, respectively (21) were used for the time-dependent inhibition part of the prediction model (Eq. 4).

greater inhibition potency towards CYP2C8 *in vitro* in comparison to gemfibrozil, whereas gemfibrozil is a more potent *in vitro* inhibitor of CYP2C9. Both gemfibrozil and its glucuronide are weak inhibitors of CYP3A4 with IC_{50} values >200 μM (Table II). The k_{deg} for CYP2C8 was calculated from the mean half-life of CYP2C8 reported by Ghanbari et al. (36), which was 23 h (range 8–41 h). The k_{inact} and K_I values for gemfibrozil glucuronide of 0.21 min^{-1} and 20 μM respectively were taken from Ogilvie *et al.* (21).

OATP1B1 inhibition assays. Cryopreserved HEK MSRII cells were thawed then washed in Dulbecco's Modified Eagle's Medium with Hams F12 nutrient mixture supplemented with 10% foetal bovine serum and 0.35 mg/ml geneticin and resuspended in the same media for plating out. Cells were seeded onto 24-well, poly-D-lysine plates at a density of 300,000 cells per well. Plates were then incubated at 37°C in an atmosphere containing 5% CO_2 for 4–6 h to allow cell adhesion. After the initial incubation period, the original media was removed and replaced with media containing OATP1B1 BacMam (37), 0.35 mg/ml geneticin and 2 mM sodium butyrate. The BacMam was added at a multiplicity of infection of 250 pfu/cell. The transduced cells were incubated for 48 h before use to allow OATP1B1 expression and a monolayer to form.

Inhibition assay. The incubation media was removed and cells were washed with 1 ml per well of Dulbecco's phosphate buffered saline (DPBS) at 37°C. The wash buffer was removed and replaced with DPBS containing test compounds. Cells were then pre-incubated in the presence of the test compound (0.01–3, 0.1–30, 0.1–100 and 0.1–100 μM for cyclosporine, repaglinide, cerivastatin and gemfibrozil, respectively) for 15–30 min. At the end of the pre-incubation period, the test compound solutions were removed and DPBS containing test compound (same concentrations as during pre-incubation) and probe substrate, [^{3}H]-estradiol glucuronide (0.02 μM), was added to each well. The DMSO concentration was constant at 0.5% throughout the experiment. The cells were then incubated for 3 min before removal of the incubation buffer and addition of 800 μl ice cold DPBS to stop further uptake. Cells were washed a further two times with ice cold DPBS. Incubations were performed in triplicate per test compound concentration (including DMSO only, 0 μM control) and triplicate incubations were also performed with known control inhibitor (rifamycin at 10 μM).

Sample preparation. The DPBS used for the final wash step was removed and 400 μl of 1% Triton X-100 was added to each well. The plates were then incubated for 30 min at 37°C to allow cell lysis. The entire content of each well was transferred to liquid scintillation vials, 10 ml scintillated fluid (Starscint) was added and the decays per minute were counted on a liquid scintillation counter.

OATP1B1 inhibition data analysis. Probe substrate uptake was expressed as fmoles/cm^2/min in the presence of the various test compound concentrations and the control inhibitor. These data were then converted to a percentage of control uptake (in the absence of test compound). Percent of control values were entered into GraFit (Version 5.0.8, Erithacus Software, UK) and IC_{50} curves generated using either a full 4-parameter fit (Eq. 6) or a modified four parameter fit with a background equal to the percent of control activity in the presence of the control inhibitor, rifamycin.

$$\%\text{control} = \frac{\text{range}}{1 + \left(\frac{[I]}{IC_{50}}\right)^{s}} + \text{background} \qquad (6)$$

where s is equal to the slope factor and the range is derived from the fitted uninhibited value minus background.

In vitro–in vivo prediction of DDIs. The average unbound plasma concentration of gemfibrozil was calculated as described by Ito *et al.* (2), using the unbound fraction in plasma of 0.05. Gemfibrozil glucuronide has been shown to accumulate 35 to 42-fold in isolated perfused rat liver by a carrier-mediated mechanism (38) and our preliminary in house studies suggest similar tendency in human hepatocytes (data not shown). Therefore, the average estimated unbound hepatic concentration of 89 μM (range of 81–97 μM) (11) was used in the metabolic prediction models (Eqs. 3 and 4). The estimated hepatic input concentrations for gemfibrozil and cyclosporine were used for the qualitative zoning of transporter DDIs. Absorption rate constants used to obtain the $[I]$in values for gemfibrozil and cyclosporine were 0.015 and 0.0339 min^{-1}, respectively. Predicted AUC ratios<2 for DDIs observed to be >2 were classed as false negative and predicted AUC ratios ≥2 for observed ratios <2 were classed as false positive interactions, on the basis of previous consensus reports (1). Predictions were classed successful if within twofold of the observed value.

RESULTS

In vivo data. The gemfibrozil *in vivo* interactions collated included 12 victim drugs, each with differing contributions from CYP3A4, CYP2C8 and CYP2C9 to their elimination (Table I). The estimated fm_{CYP3A4} values ranged from 0.3–0.99 for pravastatin and simvastatin, respectively. A similar threefold range was observed for the estimated contribution of CYP2C9, as exemplified by rosuvastatin and glimepiride. However, the maximal contribution of CYP2C8 to the overall elimination was estimated to be 63% in the case of pioglitazone. The statin drugs are known to undergo interconversion between their acid and lactone forms which confounds estimation of fm_{CYP}. Classifying these studies according to Bjornsson *et al.* (39) indicated that 42% of the DDIs were moderate (increase in AUC twofold to fivefold), 17% within the range of potent inhibition (AUCi/AUC >5) and the remaining 42% were weak (AUCi/AUC ≤2). The mean fold increase in AUC in the presence of gemfibrozil ranged from no change up to eightfold, in case of zopiclone and repaglinide, respectively (Fig. 1A, Table I).

The relationship between the changes in volume of distribution and clearance for 11 victim drugs in the presence of gemfibrozil is shown in Fig. 1B. The decrease in clearance ranged from 1–88%, in comparison to the 3–65% decrease in volume, with zopiclone showing the smallest and repaglinide the greatest decrease in both parameters. Most of the substrates showed a greater decrease in clearance compared to volume, with the exception of pravastatin and atorvastatin. Pravastatin is mostly excreted unchanged (estimated fm_{CYP3A4}

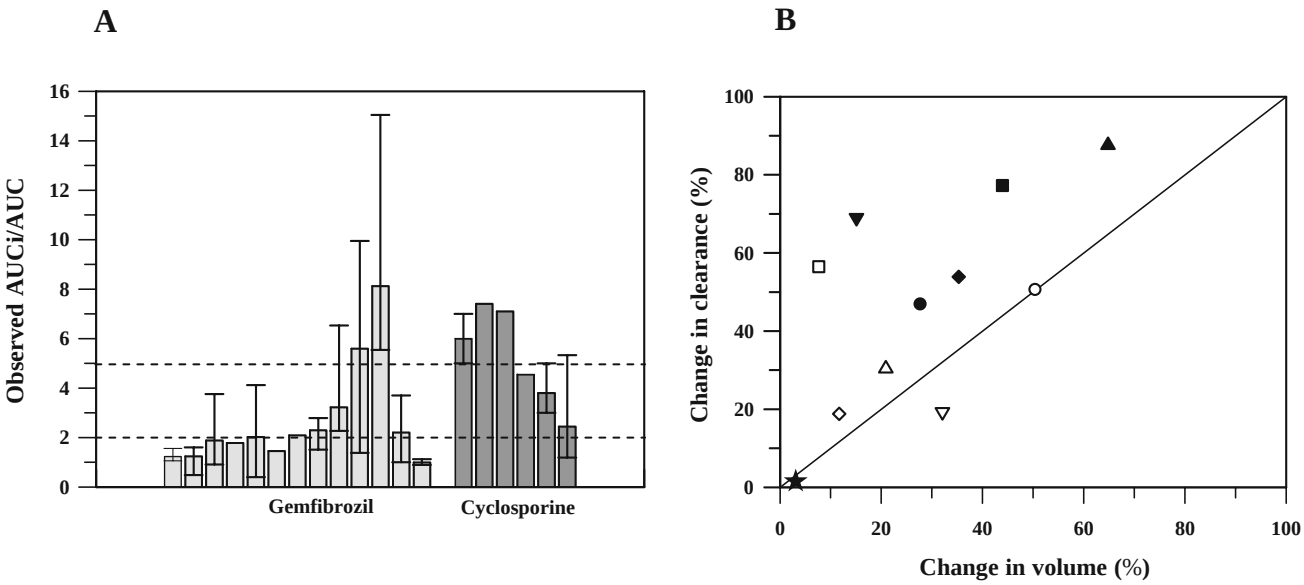

Fig. 1. **A** Assessment of gemfibrozil and cyclosporine inhibitory potential *in vivo*. Classification of 19 gemfibrozil (*light grey bars*) and cyclosporine (*dark grey bars*) DDIs according to Bjornsson *et al.* (37) where AUCi/AUC > 5 indicate potent, $2 < AUC_i/AUC < 5$ moderate and $AUC_i/AUC \leq 2$ weak interactions. The order of victim drugs in gemfibrozil DDIs is glimepiride, atorvastatin, rosuvastatin, lovastatin, pravastatin, pitavastatin, simvastatin, rosiglitazone, pioglitazone, cerivastatin, repaglinide, loperamide and zopiclone, the details are in Table I (15–17,19,20,26–33,40). Pravastatin, atorvastatin, rosuvastatin, pitavastatin, cerivastatin and repaglinide were victim drugs in cyclosporine DDIs (41–46). *Error bars* represent a range of the observed AUC ratios *in vivo* (when reported in the clinical study). **B** Changes in the V/F and CL for 11 substrates investigated after the multiple dosing of gemfibrozil. Different substrates are identified: *filled squares* represent cerivastatin, *open triangles* simvastatin, *filled circles* rosuvastatin, *open circles* pravastatin, *filled triangles* repaglinide, *open squares* rosiglitazone, *filled inverted triangles* pioglitazone, *open diamonds* glimepiride, *open inverted triangles* atorvastatin, *filled diamonds* loperamide and *filled stars* zopiclone.

0.31) (47); therefore, the gemfibrozil interaction is likely to be only at the level of transporters, resulting in an equal decrease in both parameters. Atorvastatin was the only substrate that showed a greater decrease in volume than in clearance. Although recent studies by Kameyama *et al.* (48) and Lau *et al.* (25,49) have confirmed the importance of hepatic uptake via OATP1B1, the effect on *V*/*F* might be a combined effect of gemfibrozil inhibition of other transporters affecting atorvastatin disposition in addition to OATP1B1. Also, any effect of the inhibitor on the bioavailability will consequently affect the volume of distribution, which may further complicate the interpretation. No trend was observed between the estimated fm_{CYPi} or physicochemical properties (log*P*) of the victim drugs and changes in these two pharmacokinetic paremeters for this group of substrates. The rank order of changes in volume did not necessarily reflect the reported affinity of victim drugs for the OATP1B1 transporter (50,51). For some of the substrates investigated, *in vitro* OATP1B1 data were not available to establish any definitive link between changes in volume and affinity towards OATP1B1.

Prediction based on the metabolic inhibition. The effect of multiple inhibitors (gemfibrozil and its glucuronide) on different metabolic enzymes (CYP2C8, CYP2C9 and CYP3A4) was incorporated into the metabolic prediction model (Eq. 3 or 4) using the corresponding *in vitro* data (Table II). An estimated mean gemfibrozil glucuronide unbound concentration in the hepatocytes of 89 μM was used (11), assuming similar extensive accumulation of gemfibrozil glucuronide in human hepatocytes to that reported in rats (38). In the case of gemfibrozil, the calculated average unbound plasma concentration was used. For the victim drugs with fm_{CYP3A4} <0.5, inhibition of this enzyme by gemfibrozil and its glucuronide was negligible and its contribution was omitted from the prediction equation (Eq. 3). Gemfibrozil-glucuronide inhibits CYP2C8 in a time-dependent manner (21); therefore, only for gemfibrozil interactions with CYP2C8 substrates (cerivastatin, pioglitazone, repaglinide, loperamide and rosiglitazone), the time-dependent component of the model (Eq. 4) was relevant. The metabolism inhibition model predicted 83% of the interaction studies within twofold of the observed values. Cerivastatin and repaglinide interactions with gemfibrozil were under-predicted by 54–76%, as shown in Fig. 2. The use of this prediction model resulted in 33% of the studies being predicted as false negatives. In contrast to the general under-prediction trend, the glimepiride interaction was over-predicted. This is probably due the lack of data available to make an accurate fm_{CYP2C9} estimate resulting in an over-estimation of the contribution of CYP2C9 (Table I). This again highlights the issue of the discrepancy in potency of gemfibrozil towards CYP2C9 *in vivo* and *in vitro* (13,27,30).

Impact of the time-dependent inhibition of CYP2C8 on the prediction of DDI. The impact of irreversible inhibition of CYP2C8 by gemfibrozil glucuronide on the predicted AUC ratio was investigated using a subset of five interactions from the database, including cerivastatin, pioglitazone, repaglinide, loperamide and rosiglitazone as victim drugs (Table I). The prediction model incorporated the effect of multiple inhibitors (i.e., gemfibrozil and its glucuronide) via independent inhibition mechanisms (Eq. 4). Estimated concentrations of gemfibrozil and its glucuronide were the same as described for the reversible prediction model using the corresponding reversible and time-dependent *in vitro* data (Table II).

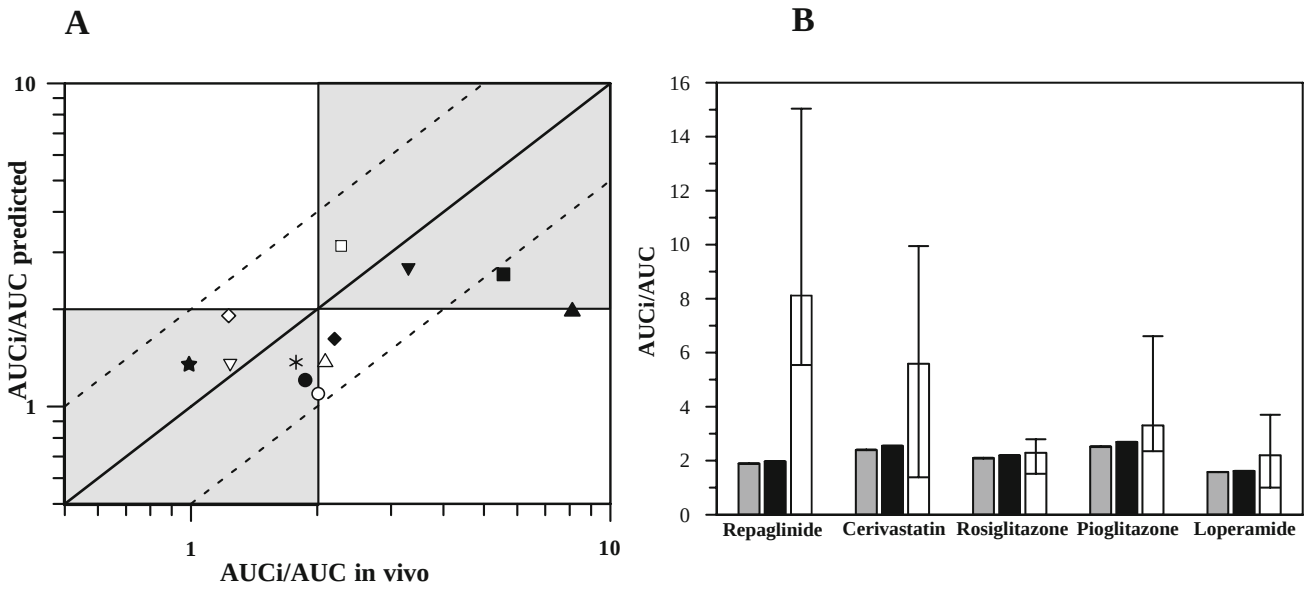

Fig. 2. Relationship between predicted and observed AUC ratios for gemfibrozil interactions. **A** Prediction of 12 DDI using Eq. 3 or 4 (CYP2C8 substrates) applying the estimated unbound concentration of gemfibrozil glucuronide in the hepatocytes (89 μM) and average unbound plasma concentration of the parent (3 μM), corresponding fm_{CYP} (Table I) and *in vitro* data (Table II). Different substrates are identified: *filled squares* represent cerivastatin, *open triangles* simvastatin, *filled circles* rosuvastatin, *asterisks* lovastatin, *open circles* pravastatin, *filled triangles* repaglinide, *open squares* rosiglitazone, *filled inverted triangles* pioglitazone, *open diamonds* glimepiride, *open inverted triangles* atorvastatin, *filled diamonds* loperamide and *filled stars* zopiclone. The *solid line* represents line of unity, whereas *dashed lines* represent the twofold limit in prediction accuracy. The shaded areas correspond to the true negative and positive drug-drug interactions defined by the twofold increase in the AUC. **B** Impact of time-dependent inhibition of CYP2C8 by gemfibrozil glucuronide on the prediction of DDIs with repaglinide, cerivastatin, rosiglitazone, pioglitazone and loperamide. *Grey bars* represent reversible prediction model (Eq. 3), *black bars* combined reversible and time-dependent effect (Eq. 4) and *white bars* observed *in vivo* interaction. Predicted range is obtained using estimated unbound concentration of gemfibrozil glucuronide in the hepatocyte of 81 to 97 μM (11).

Application of the combined reversible and time-dependent prediction model showed only a marginal effect on the predicted magnitude of the DDIs (Fig. 2B). The extent of under-prediction was comparable to the reversible metabolic model as only a minor reduction in under-prediction (1–3%) of repaglinide and cerivastatin interactions was observed. Varying the CYP2C8 degradation half-life from 8 to 41 hours ($k_{deg} = 0.0005–0.00144$ min^{-1} (36)) or the *in vitro* parameters for the TDI model (e.g., K_I from 20 to 52 μM as reported by Ogilvie *et al.* (21)) had no significant effect on the predicted AUC ratio.

The effect of increasing fm_{CYP2C8} (0.1–1) and inhibitor (gemfibrozil glucuronide) concentration on the predicted extent of interactions using either the reversible or the combined reversible and TDI model is shown in Fig. 3A and B, respectively. The simulation confirms the insensitivity of predictions to the model applied for substrates with an fm_{CYP2C8} <0.65 (as estimated for victim drugs investigated here, Table I), when an estimated gemfibrozil glucuronide concentration of 89 μM was used. However, the TDI model showed greater sensitivity at lower concentrations of gemfibrozil glucuronide for substrates with a greater contribution of CYP2C8 to the overall elimination. This is illustrated by the 270%, 340% and 130% higher predicted AUC ratios with the TDI model in comparison to the reversible model at gemfibrozil glucuronide concentrations of 0.1, 10 and 100 μM, respectively when the $fm_{CYP2C8} = 0.9$.

OATP1B1 in vitro inhibition data. Inhibition of OATP1B1 transporter expressed in HEK293 cells was assessed using ^{3}H-estradiol glucuronide (0.02 μM) as the probe substrate. The IC_{50} plots for cyclosporine, gemfibrozil, repaglinide and cerivastatin are shown in Fig. 4. A 100-fold range in the potency was observed, with the following rank order—cyclosporine > repaglinide > cerivastatin > gemfibrozil and the IC_{50} values of 0.05 ± 0.005, 0.32 ± 0.02, 1.7 ± 0.5 and 7.4 ± 1.3 μM, respectively. Gemfibrozil was found to be a 10-fold more potent inhibitor compared to the previously reported estimate obtained in Madin Darby canine kidney cells ($IC_{50} = 72.4$ μM, (11)).

Qualitative zoning of transporter DDIs. The *in vitro* OATP1B1 inhibition data obtained in HEK293 cells were used to evaluate $[I]in/K_i$ ratio to qualitatively zone 14 potentially transporter-related gemfibrozil and cyclosporine drug–drug interactions, as shown in Fig. 5. In the case of pravastatin, atorvastatin, rosuvastatin and pitavastatin, DDIs with cyclosporine were in the range of medium to potent (4.6 to 7.4-fold increase), whereas gemfibrozil caused only a minor increase in the AUC for the same victim drugs (1.45 to 2-fold for pitavastatin and pravastatin, respectively) (Fig. 1A). However, the opposite was the case for DDIs with repaglinide and cerivastatin, where the magnitude of interaction was far more pronounced in the presence of gemfibrozil, indicating the importance of a metabolic inhibition mechanism as well.

The use of $[I]in$ resulted in essentially no false negative predictions, though 4/14 predictions were false positives. In addition, most of the true positive interactions were significantly over-predicted (3 to 17 and 20 to 39-fold for gemfibrozil and

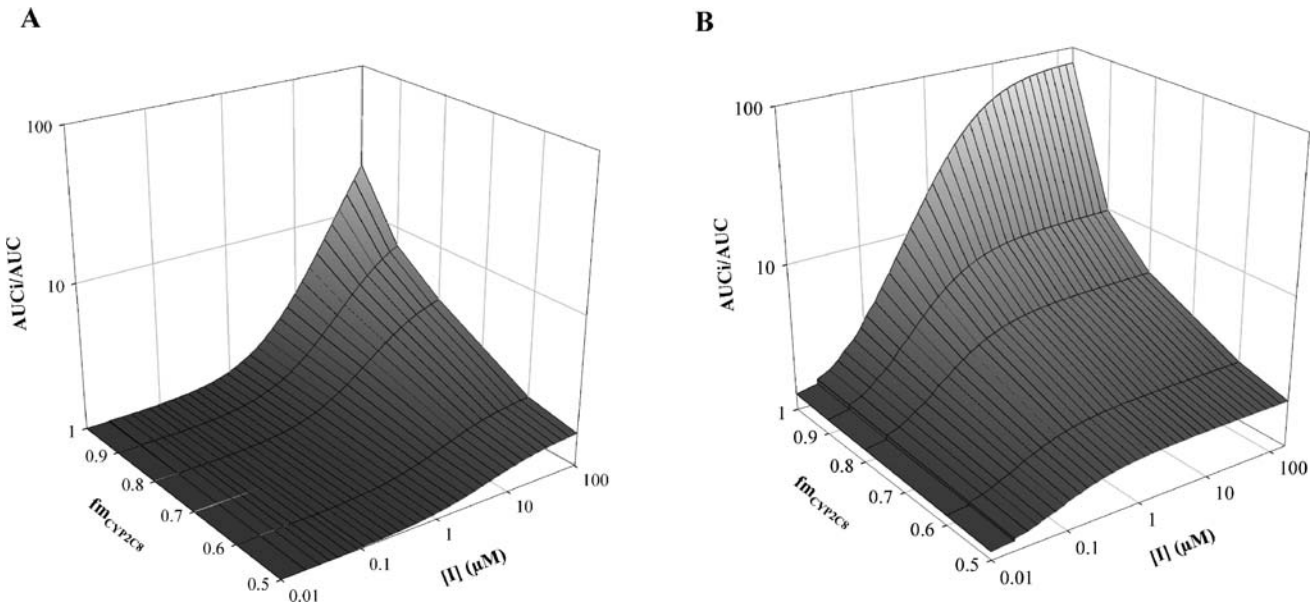

Fig. 3. Utility of reversible and irreversible prediction model for substrates with differential contribution of CYP2C8 to the overall elimination. The sensitivity of the predicted AUC ratios on fm_{CYP2C8} (0.1–1) over a range of inhibitor concentrations applying the reversible (**A**) and combined reversible and time-dependent prediction model (**B**).

cyclosporine DDIs, respectively). DDIs with atorvastatin as a victim drug were significantly over-predicted with both inhibitors (17 and 34-fold for gemfibrozil and cyclosporine DDIs, respectively). In contrast to the metabolic models, where repaglinide and cerivastatin interactions were under-predicted, this approach over-predicted the extent of the observed DDIs by 2.7 to 4-fold, respectively. Figure 5 illustrates the consequences of the lack of a substrate specific term in the transporter model, as the predicted $[I]in/K_i$ ratios fall in a flat line in case of gemfibrozil (same inhibitor dosing regimen, same *in vitro* K_i).

In order to address the differential contribution of OATP1B1 in the disposition of the various victim drugs, the transporter model has been refined to incorporate fraction of drug transported (ft) in the prediction equation (Appendix, Eq. 12). Figure 6 illustrates that the addition of the ft term has a marked impact on the predicted AUC ratio. This would be of particular relevance for the assessment of interaction potential of potent OATP1B1 inhibitors, e.g., cyclosporine (11), telmisartan and ritonavir (23). For example, in the case of the pitavastatin–cyclosporine interaction, the use of ft of 0.8 (estimated contribution of OATP1B1 to pitavastatin hepatic uptake ranges from 75% to 86% (53)) predicts a 3.3-fold increase in pitavastatin AUC. The predicted value is in a very good agreement with a 4.5-fold AUC increase observed *in vivo* (44), whereas a value of 1 results in over-prediction of this DDI by fivefold.

DISCUSSION

In the assessment of DDIs, the contribution of multiple inhibitors (or metabolites) and/or the consequence of multiple inhibition mechanisms is rarely included (8,54). The current study focuses on this issue and describes a systematic analysis of metabolic interactions involving gemfibrozil and its glucuronide as reversible and time-dependent inhibitors of CYP2C8, respectively. In addition, inhibition of the hepatic uptake transporter OATP1B1 and its significance to the magnitude of several DDIs is assessed.

Importance of reversible and irreversible inhibition of CYP2C8. Ogilvie *et al.* (21) demonstrated the TDI potential of gemfibrozil glucuronide *in vitro* and suggested that incorporating the irreversible inhibition of CYP2C8 into a prediction model would enable a more accurate prediction of gemfibrozil DDIs. However, this situation would only be valid for victim drugs eliminated predominantly via CYP2C8 ($fm_{CYP2C8} > 0.8$), which is not the case for the drugs with the reported interaction with gemfibrozil to date (Table I). The current best estimates of the contribution of CYP2C8 to the overall elimination of the victim drugs in the database do not exceed 65% (pioglitazone). Therefore, at these lower fm_{CYP2C8} values the incorporation of the irreversible inhibition mechanism into the model (Eq. 4) shows no significant improvement compared to the simple reversible prediction model (Eq. 3). In addition, gemfibrozil glucuronide is not an exceptionally potent time-dependent inhibitor of CYP2C8 (20-fold less potent compared to phenelzine (52)). Therefore, the use of the TDI model does not result in very high predictions, unless a victim drug has a high fm_{CYP2C8}. The sensitivity of the metabolic model to fm_{CYP2C8} for different inhibition mechanisms is illustrated in Fig. 3 and is consistent with previous reports (7,8,55). Figure 3 also illustrates the importance of the inhibitor concentration to the predicted outcome and this may be further complicated by the pharmacokinetics of the inhibitor and the differential dosing interval between inhibitor dose and victim drug administration.

Importance of multiple inhibitors. When two inhibitors act via the same mechanism, the effect of the less potent inhibitor in the prediction model may be minor, in particular

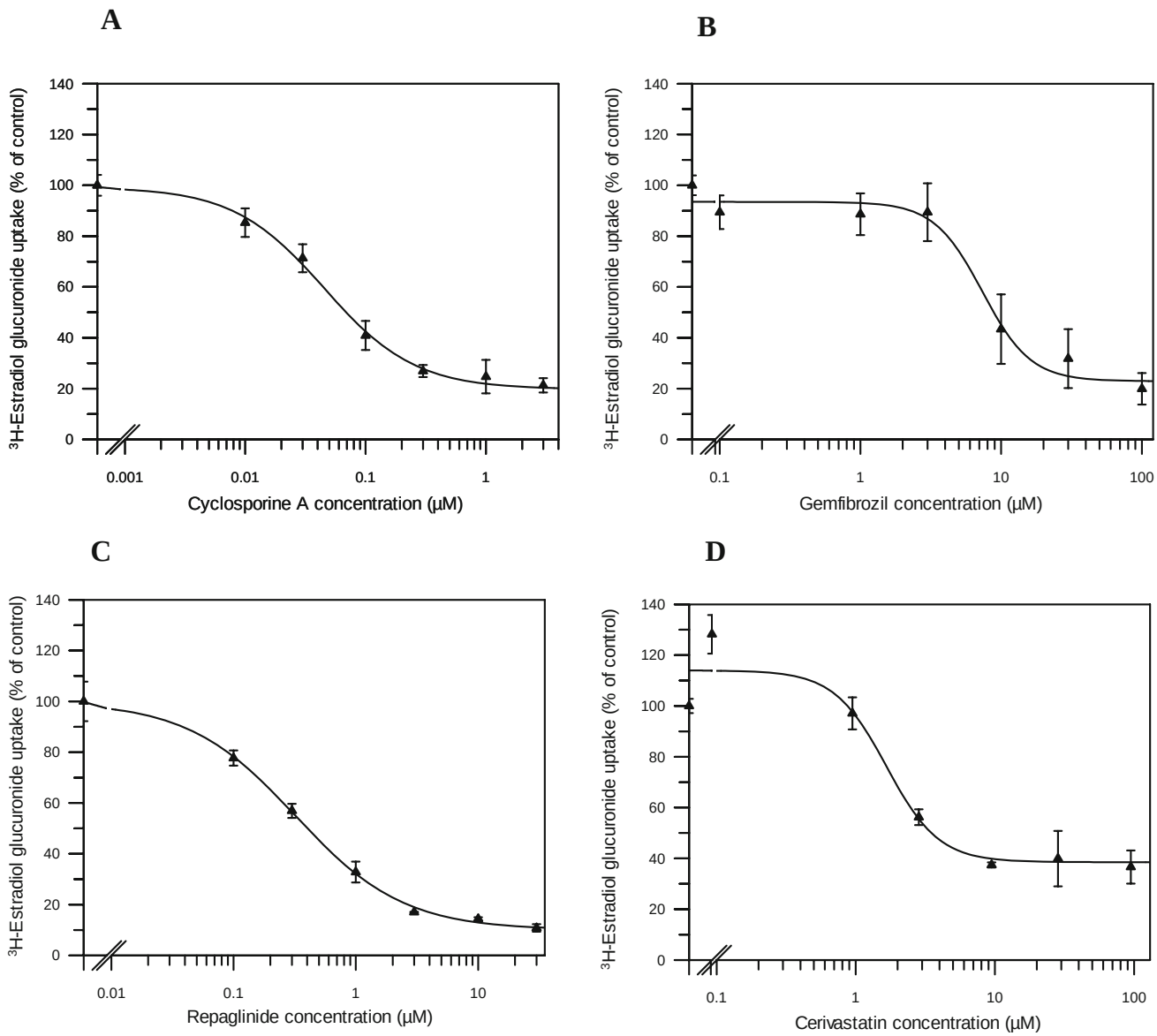

Fig. 4. IC_{50} plots for cyclosporine (**A**), gemfibrozil (**B**), repaglinide (**C**) and cerivastatin (**D**). Experiments were performed in HEK293 cells expressing the OATP1B1 transporter using ^{3}H-estradiol glucuronide (0.02 μM) as the probe substrate. Data represent mean±SD ($n = 3$).

if the relative ratio of I/K_i of two inhibitors is >100-fold, as in the case of gemfibrozil and its glucuronide. Therefore, in such cases it would be sufficient to include only the more potent inhibitor in the prediction model. The non-additive effect of multiple inhibitors is not exclusive to the reversible inhibition mechanism and has been illustrated previously with irreversible interactions (8). There is a perception that a greater combined effect is expected for inhibitors that act via different pathways (P450s) or independent mechanisms (e.g., reversible and irreversible as in case of gemfibrozil and its acyl-glucuronide). However, the current study shows that in cases when the contribution of the inhibited second enzyme is less than 50% (e.g., CYP3A4 in case of repaglinide), its contribution to the overall effect will be negligible. However, inhibition of one P450 enzyme by a potent inhibitor (e.g., CYP2C8 by gemfibrozil glucuronide) may shift the fm_{CYPi} balance towards a different P450 (e.g., CYP3A4), which may explain the magnitude of the effect observed in itraconazole–gemfibrozil interaction with repaglinide (16) and loperamide (32) and the smaller effect when itraconazole is administered alone. The effect of multiple inhibitors on the fm_{CYPi} balance is dependent on the relative potency and concentration of each of the inhibitor.

Importance of intestinal inhibition. Simvastatin, atorvastatin and lovastatin represent the only victim drugs in the database where CYP3A4 contributes more than 50% to elimination and where an interaction in the gut wall may be expected in the presence of an inhibitor. Although the estimated intestinal extraction for these three statins varies from 34–76% (8,56), the impact of gemfibrozil on their intestinal first-pass metabolism can be considered negligible due to its weak potency towards CYP3A4 (Table II). The same minimal decrease in the intestinal clearance in the presence of gemfibrozil can be expected for the repaglinide interaction.

Importance of OATP1B1 interaction. The analysis of changes in the volume and clearance in the presence of

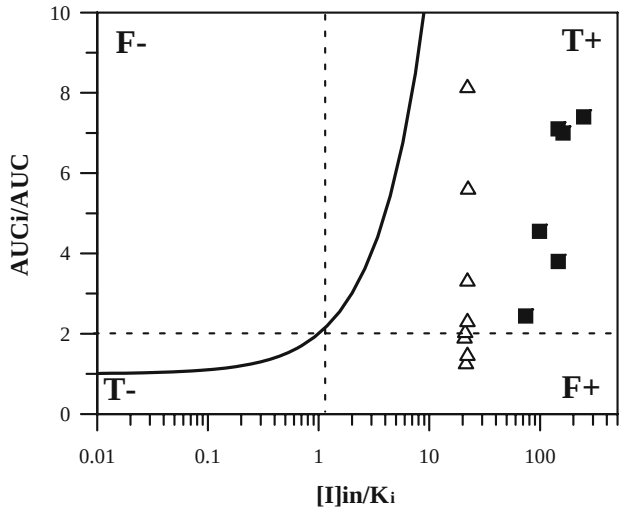

Fig. 5. Qualitative zoning of 14 OATP1B1 DDIs using $[I]in/K_i$ approach. *Open triangles* represent gemfibrozil DDIs ($n=8$), *filled squares* cyclosporine DDIs ($n=6$) shown in Table I and Fig. 1a, respectively. F+ and F− indicate the false positive and false negative predictions, respectively.

gemfibrozil indicated that for many of the victim drugs, the interaction was partly transporter-mediated (Fig. 1B). The metabolic models tested were unable to account for the extent of interaction with some drugs (particularly repaglinide, cerivastatin and pioglitazone) and indicated the need to investigate the utility of a transporter model for prediction of these DDIs. The $[I]in/K_i$ ratio was evaluated for qualitative zoning of 14 hepatic uptake transporter-mediated gemfibrozil and cyclosporine DDIs using *in vitro* inhibition data obtained in HEK293 cells (Figs. 4 and 5). The rationale for qualitative zoning was the increasing concern over potential transporter-related DDIs in the early stages of the drug development (57) and the question whether this empirical approach can facilitate the decision on the necessity of a follow up clinical study.

Qualitative zoning resulted in no false negative predictions; however, the extent of observed gemfibrozil and cyclosporine interactions was significantly over-predicted (Fig. 5). A number of factors may contribute to this overestimation of the impact of OATP1B1 inhibition to the overall DDI observed. Qualitative zoning is based entirely on inhibitor-related data and does not take into account the relative affinity of the substrate for the transporter(s) or the degree of reliance of the substrate on the transporter for entry into the hepatocytes, as this type of information would not be available in the early stages of drug development. This approach does not address the consequences of several transporters (e.g., OATP1B1, OATP1B3) contributing to the disposition of victim drugs, as is the case for most of the statins (23,51). In order to address the differential contribution of OATP1B1 to the victim drug disposition we proposed the use of the term fraction of drug transported (ft) in the prediction equation (Appendix, Eq. 12). This would prevent the occurrence of false positive predictions for victim drugs that may be good OATP1B1 substrates *in vitro*, but do not require major OATP1B1 involvement *in vivo*, as hepatic uptake is not the critical step in the overall clearance. Figure 6 illustrates that even minor changes in ft (i.e., changes in transporter contribution from 100% to 80%) have a significant effect on the predicted AUC ratio in a similar manner to the effect of fm_{CYPi} on the metabolic models (5,7,8). However, assigning an ft value is not straightforward. One approach is to estimate the contribution of each transporter to the total hepatic uptake *in vitro*. This can be done by comparing the hepatic uptake of a compound investigated to the uptake of a selective reference compound (e.g., estrone 3-sulfate for OATP1B1 (53)) in the transporter-expressing cell lines (e.g., HEK293) to human hepatocytes, as suggested recently (23,58). The relative activity factor obtained from this comparison can then be used to estimate the contribution of the specific transporter to total uptake. This approach estimated 75% to 86% contribution of OATP1B1 to pitavastatin hepatic uptake, which resulted in prediction of gemfibrozil and cyclosporine DDIs within twofold of *in vivo* values. Alternatively, ranking substrates for their affinity to the transporter in comparison to a representative probe substrate might prove to be useful. The OATP1B1 pharmacogenetic studies allowing comparison of transporter variants may represent a potentially useful approach to estimate ft, in an analogous manner to estimation of fm_{CYP2D6} from poor and extensive metabolisers (7).

Conclusion. This study describes a systematic analysis of effect of multiple inhibitors and different inhibition mechanisms on the prediction of gemfibrozil and cyclosporine interactions. Although gemfibrozil glucuronide is a time-dependent inhibitor of CYP2C8 *in vitro*, a combined reversible (gemfibrozil) and time-dependent (gemfibrozil glucuronide) model was not necessary to predict the DDIs observed. The improvement in the prediction was insignificant compared to the simpler reversible inhibition model, as the estimated contribution of CYP2C8 to the overall elimination of the substrates investigated here was ≤65%. Large inter-individual variability in the observed increase in the AUC in the presence of gemfibrozil (Fig. 1A) represents an additional confounding factor. Part of this variability may

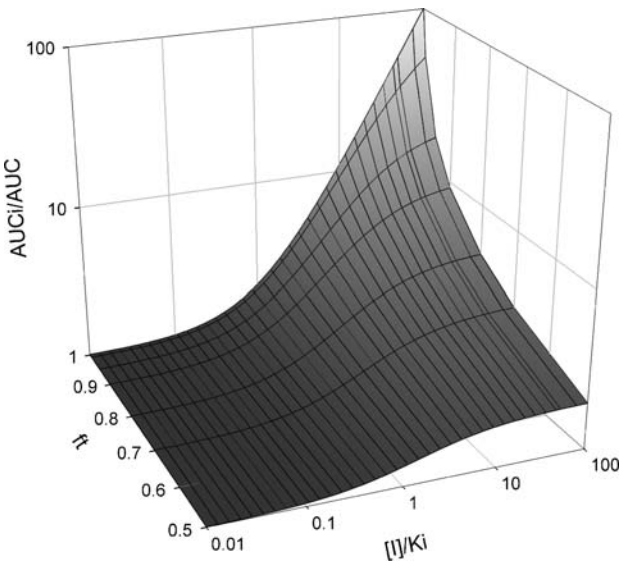

Fig. 6. Effect of ft on transporter model predictions. The sensitivity of the predicted AUC ratios on the fraction of the drug transported (ft) over a range of inhibitor potency defined by I/K_i (Appendix, Eq. 12).

be related to differences in the extent of conversion to the more potent inhibitor gemfibrozil glucuronide and the degree of glucuronide accumulation in hepatocytes. In addition, substantial variability can also be associated with some of the victim drugs—for example Niemi *et al.* (22) have recently shown the importance of SLCO1B1 polymorphisms on the pharmacokinetics of repaglinide. This may contribute to the different magnitude of DDI observed, not only in the case of this victim drug, but also for other OATP1B1 substrates (e.g., pravastatin, pitavastatin, rosuvastatin) (23,24,50,59,60).

Analogous to the reversible metabolic interactions, qualitative zoning of OATP1B1 inhibitors based on $[I]in/K_i$ can be valuable, particularly in drug screening where false negative predictions are to be avoided. However, this approach is not quantitative and false positives and over-prediction of the magnitude of a DDI may result and additional, more comprehensive studies would be required in case of positive prediction. Incorporation of the relative contribution of a particular transporter in the form of ft refines the transporter prediction model. It is anticipated that an expansion of the *in vitro* transporter database in subsequent years will allow further evaluation of this approach. A combined physiologically-based model incorporating both the inhibition of the hepatic uptake transporter and P450 metabolic pathways in a sequential manner would represent the most comprehensive prediction tool and the need for such refinement is becoming more obvious with the disposition characteristics of recently developed drugs.

ACKNOWLEDGEMENT

The authors would like to thank Dr Kathryn Kenworthy and Mrs Jennifer Thomas (GlaxoSmithKline, Ware, UK) for their help with the OATP1B1 inhibition assay.

The work was funded by a consortium of pharmaceutical companies (GlaxoSmithKline, Lilly, Novartis, Pfizer and Servier) within the Centre for Applied Pharmacokinetic Research at the University of Manchester. Part of this study was presented at the 9th ISSX Meeting, June 4–7, 2006, Manchester, UK.

APPENDIX

Total hepatic clearance can be described by Eq. 7 (58,61,62):

$$CL_{int,all} = PS_{inf\ lux} \times \frac{CL_{int}}{PS_{efflux} + CL_{int}} \quad (7)$$

where PS_{influx} and PS_{efflux} are the membrane permeability–surface area products of a drug across the sinusoidal membrane, for the influx and efflux processes, respectively, and CL_{int} is the intrinsic clearance representing both metabolic and biliary excretion of the drug. When $PS_{efflux} << CL_{int}$, $CL_{int,all} = PS_{influx}$. PS_{influx} can also be described as the clearance due to influx into the cell (CL_{influx}) (62).

When the uptake of a drug involves more than one transporter, the total influx clearance can be defined as the sum of the ratios of the Michaelis–Menten parameters for the individual transporters, assuming linear kinetics (substrate concentration $<<K_m$), as shown in Eq. 8:

$$CL_{influx} = \frac{V_{max1}}{K_{m1}} + \frac{V_{max2}}{K_{m2}} = ft_{OATP1B1} CL_{influx} + (1 - ft_{OATP1B1}) CL_{influx} \quad (8)$$

where 1 and 2 refer to influx via a particular transporter (e.g., OATP1B1). The term $ft_{OATP1B1}$ refers to the fraction of the drug transported by way of the OATP1B1 transporter, whereas the remaining fraction is transported by unspecified routes.

Influx clearance in the presence of a competitive inhibitor of OATP1B1 ($CL_{influx\ i}$) or 2 inhibitors acting via the same mechanism is shown in Eqs. 9 and 10, respectively:

$$CL_{influx}i = \frac{V_{max1}}{K_{m1}(1 + [I]/K_i)} + \frac{V_{max2}}{K_{m2}} \quad (9)$$

$$CL_{influx}i = \frac{V_{max1}}{K_{m1}(1 + [I]/K_{i1} + [I]/K_{i2})} + (1 - ft_{OATP1B1}) CL_{influx} \quad (10)$$

Combining Eqs. 8 and 10 gives:

$$CL_{influx}i = \frac{ft_{OATP1B1}\, CL_{influx}}{1 + \sum_{j}^{n} [I]j/Ki,j} + (1 - ft_{OATP1B1}) CL_{influx} \quad (11)$$

Assuming competitive inhibition and that the other transport processes are unaffected by the inhibitor, the AUC ratio is given by the following equation:

$$\frac{AUCi}{AUC} = \frac{CL_{influx}}{CL_{influx}i} = \frac{1}{\frac{ft_{OATP1B1}}{1 + \sum_{j}^{n} [I]j/Ki,j} + (1 - ft_{OATP1B1})} \quad (12)$$

REFERENCES

1. G. T. Tucker, J. B. Houston, and S. M. Huang. Optimizing drug development: strategies to assess drug metabolism/transporter interaction potential—towards a consensus. *Br. J. Clin. Pharmacol.* **52**(1):107–117 (2001).
2. K. Ito, H. S. Brown, and J. B. Houston. Database analyses for the prediction of *in vivo* drug–drug interactions from *in vitro* data. *Br. J. Clin. Pharmacol.* **57**(4):473–486 (2004).
3. A. Rostami-Hodjegan and G. Tucker. 'In silico' simulations to assess the '*in vivo*' consequences of '*in vitro*' metabolic drug–drug interactions. *Drug Discov. Today* **1**(4):441–448 (2004).
4. Y. H. Wang, D. R. Jones, and S. D. Hall. Prediction of cytochrome P450 3A inhibition by verapamil enantiomers and their metabolites. *Drug Metab. Dispos.* **32**(2):259–266 (2004).
5. H. S. Brown, K. Ito, A. Galetin, and J. B. Houston. Prediction of *in vivo* drug–drug interactions from *in vitro* data: impact of incorporating parallel pathways of drug elimination and inhibitor absorption rate constant. *Br. J. Clin. Pharmacol.* **60**(5):508–518 (2005).
6. A. Galetin, K. Ito, D. Hallifax, and J. B. Houston. CYP3A4 substrate selection and substitution in the prediction of potential drug–drug interactions. *J. Pharmacol. Exp. Ther.* **314**(1):180–190 (2005).
7. K. Ito, D. Hallifax, R. S. Obach, and J. B. Houston. Impact of parallel pathways of drug elimination and multiple cytochrome

P450 involvement on drug–drug interactions: CYP2D6 paradigm. *Drug Metab. Dispos.* **33**(6):837–844 (2005).
8. A. Galetin, H. Burt, L. Gibbons, and J. B. Houston. Prediction of time-dependent CYP3A4 drug–drug interactions: impact of enzyme degradation, parallel elimination pathways, and intestinal inhibition. *Drug Metab. Dispos.* **34**(1):166–175 (2006).
9. R. S. Obach, R. L. Walsky, K. Venkatakrishnan, E. A. Gaman, J. B. Houston, and L. M. Tremaine. The utility of *in vitro* cytochrome P450 inhibition data in the prediction of drug–drug interactions. *J. Pharmacol. Exp. Ther.* **316**(1):336–348 (2006).
10. J. S. Wang, M. Neuvonen, X. Wen, J. T. Backman, and P. J. Neuvonen. Gemfibrozil inhibits CYP2C8-mediated cerivastatin metabolism in human liver microsomes. *Drug Metab. Dispos.* **30**(12):1352–1356 (2002).
11. Y. Shitara, M. Hirano, H. Sato and Y. Sugiyama. Gemfibrozil and its glucuronide inhibit the organic anion transporting polypeptide 2 (OATP2/OATP1B1:SLC21A6)-mediated hepatic uptake and CYP2C8-mediated metabolism of cerivastatin: analysis of the mechanism of the clinically relevant drug–drug interaction between cerivastatin and gemfibrozil. *J. Pharmacol. Exp. Ther.* **311**(1):228–236 (2004).
12. L. I. Kajosaari, J. Laitila, P. J. Neuvonen, and J. T. Backman. Metabolism of repaglinide by CYP2C8 and CYP3A4 *in vitro*: effect of fibrates and rifampicin. *Basic Clin. Pharmacol. Toxicol.* **97**(4):249–256 (2005).
13. X. Wen, J. S. Wang, J. T. Backman, K. T. Kivisto, and P. J. Neuvonen. Gemfibrozil is a potent inhibitor of human cytochrome P450 2C9. *Drug Metab. Dispos.* **29**(11):1359–1361 (2001).
14. T. Prueksaritanont, C. Tang, Y. Qiu, L. Mu, R. Subramanian, and J. H. Lin. Effects of fibrates on metabolism of statins in human hepatocytes. *Drug Metab. Dispos.* **30**(11):1280–1287 (2002).
15. J. T. Backman, C. Kyrklund, M. Neuvonen, and P. J. Neuvonen. Gemfibrozil greatly increases plasma concentrations of cerivastatin. *Clin. Pharmacol. Ther.* **72**(6):685–691 (2002).
16. M. Niemi, J. T. Backman, M. Neuvonen, and P. J. Neuvonen. Effects of gemfibrozil, itraconazole, and their combination on the pharmacokinetics and pharmacodynamics of repaglinide: potentially hazardous interaction between gemfibrozil and repaglinide. *Diabetologia* **46**(3):347–351 (2003).
17. D. W. Schneck, B. K. Birmingham, J. A. Zalikowski, P. D. Mitchell, Y. Wang, P. D. Martin, K. C. Lasseter, C. D. Brown, A. S. Windass, and A. Raza. The effect of gemfibrozil on the pharmacokinetics of rosuvastatin. *Clin. Pharmacol. Ther.* **75**(5):455–463 (2004).
18. J. J. Lilja, J. T. Backman, and P. J. Neuvonen. Effect of gemfibrozil on the pharmacokinetics and pharmacodynamics of racemic warfarin in healthy subjects. *Br. J. Clin. Pharmacol.* **59**(4):433–439 (2005).
19. M. Niemi, P. J. Neuvonen, and K. T. Kivisto. Effect of gemfibrozil on the pharmacokinetics and pharmacodynamics of glimepiride. *Clin. Pharmacol. Ther.* **70**(5):439–445 (2001).
20. J. T. Backman, H. Luurila, M. Neuvonen, and P. J. Neuvonen. Rifampin markedly decreases and gemfibrozil increases the plasma concentrations of atorvastatin and its metabolites. *Clin. Pharmacol. Ther.* **78**(2):154–167 (2005).
21. B. W. Ogilvie, D. Zhang, W. Li, A. D. Rodrigues, A. E. Gipson, J. Holsapple, P. Toren, and A. Parkinson. Glucuronidation converts gemfibrozil to a potent, metabolism-dependent inhibitor of CYP2C8: implications for drug–drug interactions. *Drug Metab. Dispos.* **34**(1):191–197 (2006).
22. M. Niemi, J. T. Backman, L. I. Kajosaari, J. B. Leathart, M. Neuvonen, A. K. Daly, M. Eichelbaum, K. T. Kivisto, and P. J. Neuvonen. Polymorphic organic anion transporting polypeptide 1B1 is a major determinant of repaglinide pharmacokinetics. *Clin. .Pharmacol. Ther.* **77**(6):468–478 (2005).
23. M. Hirano, K. Maeda, Y. Shitara, and Y. Sugiyama. Drug–drug interaction between pitavastatin and various drugs via oatp1b1. *Drug Metab. Dispos.* **34**(7):1229–1236 (2006).
24. K. Maeda, I. Ieiri, K. Yasuda, A. Fujino, H. Fujiwara, K. Otsubo, M. Hirano, T. Watanabe, Y. Kitamura, K. Kusuhara, and Y. Sugiyama. Effects of organic anion transporting polypeptide 1B1 haplotype on pharmacokinetics of pravastatin, valsartan, and temocapril. *Clin. Pharmacol. Ther.* **79**(5):427–439 (2006).
25. Y. Y. Lau, Y. Huang, L. Frassetto, and L. Z. Benet. Effect of OATP1B transporter inhibition on the pharmacokinetics of atorvastatin in healthy volunteers. *Clin. Pharmacol. Ther.* **81**(2):194–204 (2007).
26. C. Kyrklund, J. T. Backman, K. T. Kivisto, M. Neuvonen, J. Laitila, and P. J. Neuvonen. Plasma concentrations of active lovastatin acid are markedly increased by gemfibrozil but not by bezafibrate. *Clin. Pharmacol. Ther.* **69**(5):340–345 (2001).
27. T. Jaakkola, J. T. Backman, M. Neuvonen, and P. J. Neuvonen. Effects of gemfibrozil, itraconazole, and their combination on the pharmacokinetics of pioglitazone. *Clin. Pharmacol. Ther.* **77**(5):404–14 (2005).
28. L. J. Deng, F. Wang, and H. D. Li. Effect of gemfibrozil on the pharmacokinetics of pioglitazone. *Eur. J. Clin. Pharmacol.* **61**(11):831–836 (2005).
29. C. Kyrklund, J. T. Backman, M. Neuvonen, and P. J. Neuvonen. Gemfibrozil increases plasma pravastatin concentrations and reduces pravastatin renal clearance. *Clin. Pharmacol. Ther.* **73**(6):538–544 (2003).
30. M. Niemi, J. T. Backman, M. Granfors, J. Laitila, M. Neuvonen, and P. J. Neuvonen. Gemfibrozil considerably increases the plasma concentrations of rosiglitazone. *Diabetologia* **46**(10):1319–1323 (2003).
31. J. T. Backman, C. Kyrklund, K. T. Kivisto, J. S. Wang, and P. J. Neuvonen. Plasma concentrations of active simvastatin acid are increased by gemfibrozil. *Clin. Pharmacol. Ther.* **68**(2):122–129 (2000).
32. M. Niemi, A. Tornio, M. K. Pasanen, H. Fredrikson, P. J. Neuvonen, and J. T. Backman. Itraconazole, gemfibrozil and their combination markedly raise the plasma concentrations of loperamide. *Eur. J. Clin. Pharmacol.* **62**:463–472 (2006).
33. A. Tornio, P. J. Neuvonen, and J. T. Backman. The CYP2C8 inhibitor gemfibrozil does not increase the plasma concentrations of zopiclone. *Eur. J. Clin. Pharmacol.* **62**:645–651 (2006).
34. T. Jaakkola, J. Laitila, P. J. Neuvonen, and J. T. Backman. Pioglitazone is metabolised by CYP2C8 and CYP3A4 *in vitro*: potential for interactions with CYP2C8 inhibitors. *Basic Clin. Pharmacol. Toxicol.* **99**:44–51 (2006).
35. K. A. Kim, J. Chung, D. H. Jung, and J. Y. Park. Identification of cytochrome P450 isoforms involved in the metabolism of loperamide in human liver microsomes. *Eur. J. Clin. Pharmacol.* **60**:575–581 (2004).
36. F. Ghanbari, K. Rowland-Yeo, J. C. Bloomer, S. E. Clarke, M. S. Lennard, G. T. Tucker, and A. Rostami-Hodjegan. A critical evaluation of the experimental design of studies of mechanism based enzyme inhibition, with implications for *in vitro–in vivo* extrapolation. *Curr. Drug Metab.* **7**(3):315–334 (2006).
37. N. J. Hassan, D. J. Pountney, C. Ellis, D. E. Mossakowska. BacMam recombinant baculovirus in transporter expression: a study of BCRP and OATP1B1. *Protein Expr. Purif.* **47**(2): 591–8 (2006).
38. L. Sabordo, B. C. Sallustio, A. M. Evans, and R. L. Nation. Hepatic disposition of the acyl glucuronide1-*O*-gemfibrozil-beta-D-glucuronide: effects of dibromosulfophthalein on membrane transport and aglycone formation. *J. Pharmacol. Exp. Ther.* **288**(2):414–420 (1999).
39. T. D. Bjornsson, J. T. Callaghan, H. J. Einolf, V. Fischer, L. Gan, S. Grimm, J. Kao, S. P. King, G. Miwa, L. Ni, G. Kumar, J. McLeod, R. S. Obach, S. Roberts, A. Roe, A. Shah, F. Snikeris, J. T. Sullivan, D. Tweedie, J. M. Vega, J. Walsh, and S. A. Wrighton. The conduct of *in vitro* and *in vivo* drug–drug interaction studies: a Pharmaceutical Research and Manufacturers of America (PhRMA) perspective. *Drug Metab. Dispos.* **31**(7):815–832 (2003).
40. P. Mathew, T. Cuddy, W. G. Tracewell, and D. Salazar. An open-label study on the pharmacokinetics (PK) of pitavastatin (NK-104) when administered concomitantly with fenofibrate or gemfibrozil in healthy volunteers. *Clin. Pharmacol. Ther.* **75**:P33–P33 (2004).
41. C. Olbricht, C. Wanner, T. Eisenhauer, V. Kliem, R. Doll, M. Boddaert, P. O'Grady, M. Krekler, B. Mangold, and U. Christians. Accumulation of lovastatin, but not pravastatin, in the blood of cyclosporine-treated kidney graft patients after multiple doses. *Clin. Pharmacol. Ther.* **62**(3):311–321 (1997).
42. A. Asberg, A. Hartmann, E. Fjeldsa, S. Bergan, and H. Holdaas. Bilateral pharmacokinetic interaction between cyclosporine A and atorvastatin in renal transplant recipients. *Am. J. Transplant.* **1**(4):382–6 (2001).

43. S. G. Simonson, A. Raza, P. D. Martin, P. D. Mitchell, J. A. Jarcho, C. D. Brown, A. S. Windass, and D. W. Schneck. Rosuvastatin pharmacokinetics in heart transplant recipients administered an antirejection regimen including cyclosporine. *Clin. Pharmacol. Ther.* **76**(2):167–177 (2004).
44. T. Hasunuma, M. Nakamura, T. Yachi, N. Arisawa, K. Fukushima, H. Iijima. The drug–drug interactions of pitavastatin (NK-104), a novel HMG-CoA reductase inhibitor and cyclosporine. *J. Clin. Ther. Med.* **19**:381–389 (2003).
45. W. Muck, I. Mai, L. Fritsche, K. Ochmann, G. Rohde, S. Unger, A. Johne, S. Bauer, K. Budde, I. Roots, H. H. Neumayer, and J. Kuhlmann. Increase in cerivastatin systemic exposure after single and multiple dosing in cyclosporine-treated kidney transplant recipients. *Clin. Pharmacol. Ther.* **65**(3):251–61 (1999).
46. L. I. Kajosaari, M. Niemi, M. Neuvonen, J. Laitila, P. J. Neuvonen, and J. T. Backman. Cyclosporine markedly raises the plasma concentrations of repaglinide. *Clin. Pharmacol. Ther.* **78**(4):388–399 (2005).
47. D. W. Everett, T. J. Chando, G. C. Didonato, S. M. Singhvi, H. Y. Pan, and S. H. Weinstein. Biotransformation of pravastatin sodium in humans. *Drug Metab. Dispos.* **19**(4):740–748 (1991).
48. Y. Kameyama, K. Yamashita, K. Kobayashi, M. Hosokawa, and K. Chiba. Functional characterization of SLCO1B1 (OATP-C) variants, SLCO1B1*5, SLCO1B1*15 and SLCO1B1*15+ C1007G, by using transient expression systems of HeLa and HEK293 cells. *Pharmacogenet. Genomics* **15**(7):513–522 (2005).
49. Y. Y. Lau, H. Okochi, Y. Huang, and L. Z. Benet. Multiple transporters affect the disposition of atorvastatin and its two active hydroxy metabolites: application of *in vitro* and ex situ systems. *J. Pharmacol. Exp. Ther.* **316**(2):762–771 (2006).
50. R. H. Ho, R. G. Tirona, B. F. Leake, H. Glaeser, W. Lee, C. J. Lemke, Y. Wang, and R. B. Kim. Drug and bile acid transporters in rosuvastatin hepatic uptake: function, expression and pharmacogenetics. *Gastroenterology* **130**:1793–1806 (2006).
51. Y. Shitara and Y. Sugiyama. Pharmacokinetic and pharmacodynamic alterations of 3-hydroxy-3-methylglutaryl coenzyme A (HMG-CoA) reductase inhibitors: drug–drug interactions and interindividual differences in transporter and metabolic enzyme functions. *Pharmacol. Ther.* **112**(1):71–105 (2006).
52. T. M. Polasek, D. J. Elliot, B. C. Lewis, and J. O. Miners. Mechanism-based inactivation of human cytochrome P450 by drugs *in vitro*. *J. Pharmacol. Exp. Ther.* **311**(3):996–1007 (2004).
53. M. Hirano, K. Maeda, Y. Shitara, and Y. Sugiyama. Contribution of OATP2 (OATP1B1) and OATP8 (OATP1B3) to the hepatic uptake of pitavastatin in humans. *J. Pharmacol. Exp. Ther.* **311**(1):139–146 (2004).
54. N. Isoherranen, K. L. Kunze, K. E. Allen, W. L. Nelson, and K. E. Thummel. Role of itraconazole metabolites in CYP3A4 inhibition. *Drug Metab. Dispos.* **32**:1121–1131 (2004).
55. J. Y. Chien, A. Lucksiri, C. S. Ernest, II, C. Gorski, S. A. Wrighton, and S. D. Hall. Stochastic prediction of CYP3A-mediated inhibition of midazolam clearance by ketoconazole. *Drug Metab. Dispos.* **34**(7):1208–1219 (2006).
56. H. Lennernas. Clinical pharmacokinetics of atorvastatin. *Clin. Pharmacokinet.* **42**:1141–1160 (2003).
57. S. M. Huang, R. Temple, D. C. Throckmorton, and L. J. Lesko. Drug interaction studies: study design, data analysis, and implications for dosing and labeling. *Clin. Pharmacol. Ther.* **81**(2):298–304 (2007).
58. Y. Shitara, T. Horie, and Y. Sugiyama. Transporters as a determinant of drug clearance and tissue distribution. *Eur. J. Pharm. Sci.* **27**(5):425–446 (2006).
59. I. Ieiri, S. Suwannakul, K. Maeda, H. Uchimaru, K. Hashimoto, M. Kimura, H. Fujino, M. Hirano, H. Kusuhara, S. Irie, S. Higuchi, and Y. Sugiyama. SLCO1B1 (OATP1B1, an uptake transporter) and ABCG2 (BCRP, an efflux transporter) variant alleles and pharmacokinetics of pitavastatin in healthy volunteers. *Clin. Pharmacol. Ther.* In press (2007)
60. K. T. Kivisto and M. Niemi. Influence of drug transporter polymorphisms on pravastatin pharmacokinetics in humans. *Pharm. Res.* **24**(2):239–47 (2007).
61. K. S. Pang and J. R. Gillette. Kinetics of metabolite formation and elimination in the perfused rat liver preparation: differences between the elimination of preformed acetaminophen and acetaminophen formed from phenacetin. *J. Pharmacol. Exp. Ther.* **207**(1):178–194 (1978).
62. L. Liu and K. S. Pang. The roles of transporters and enzymes in hepatic drug processing. *Drug Metab. Dispos.* **33**(1):1–9 (2005).